

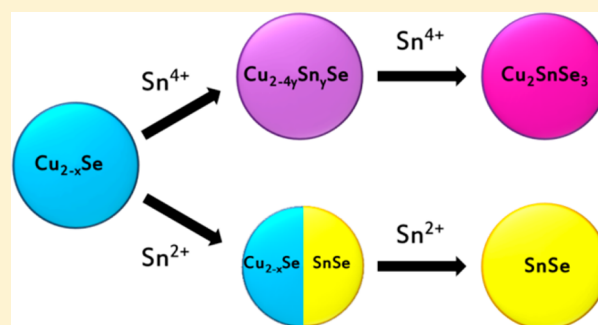
Sn Cation Valency Dependence in Cation Exchange Reactions Involving Cu_{2-x}Se Nanocrystals

Luca De Trizio,[†] Hongbo Li,[†] Alberto Casu,[†] Alessandro Genovese,[†] Ayyappan Sathya,[†] Gabriele C. Messina,[‡] and Liberato Manna^{*,†}

[†]Department of Nanochemistry and [‡]Department of Nanostructures, Istituto Italiano di Tecnologia (IIT), via Morego, 30, 16163 Genova, Italy

S Supporting Information

ABSTRACT: We studied cation exchange reactions in colloidal Cu_{2-x}Se nanocrystals (NCs) involving the replacement of Cu^+ cations with either Sn^{2+} or Sn^{4+} cations. This is a model system in several aspects: first, the +2 and +4 oxidation states for tin are relatively stable; in addition, the phase of the Cu_{2-x}Se NCs remains cubic regardless of the degree of copper deficiency (that is, “ x ”) in the NC lattice. Also, Sn^{4+} ions are comparable in size to the Cu^+ ions, while Sn^{2+} ones are much larger. We show here that the valency of the entering Sn ions dictates the structure and composition not only of the final products but also of the intermediate steps of the exchange. When Sn^{4+} cations are used, alloyed $\text{Cu}_{2-4y}\text{Sn}_y\text{Se}$ NCs (with $y \leq 0.33$) are formed as intermediates, with almost no distortion of the anion framework, apart from a small contraction. In this exchange reaction the final stoichiometry of the NCs cannot go beyond $\text{Cu}_{0.66}\text{Sn}_{0.33}\text{Se}$ (that is Cu_2SnSe_3), as any further replacement of Cu^+ cations with Sn^{4+} cations would require a drastic reorganization of the anion framework, which is not possible at the reaction conditions of the experiments. When instead Sn^{2+} cations are employed, SnSe NCs are formed, mostly in the orthorhombic phase, with significant, albeit not drastic, distortion of the anion framework. Intermediate steps in this exchange reaction are represented by Janus-type $\text{Cu}_{2-x}\text{Se}/\text{SnSe}$ heterostructures, with no Cu-Sn-Se alloys.



INTRODUCTION

Research on colloidal inorganic nanocrystals (NCs) has gone through much advancement in the past 15 years,¹ especially in synthesis,^{2–4} in assembly,⁵ and in the control of their surface chemistry,⁶ which has uncovered new scenarios for the use of NCs in many areas.⁷ An emerging field of research is the study of chemical transformations in NCs,⁸ above all cation exchange^{9–16} which allows for the substitution of the original cations with new desired ones with preservation (or slight reorganization) of the anion framework. The great importance of these reactions relies on the possibility to follow established traditional hot-injection routes to synthesize NCs with well-defined size, shape, composition, and crystal structure, and to use them as anion scaffolds for the preparation of new NCs that currently cannot be accessed through a direct synthesis.^{9–12,17,18}

Cation exchange reactions have additionally been shown to take place even in elaborate crystal structures, such as core-shell ones, opening up new horizons in the fabrication of novel types of nanoheterostructures.^{12–14,19–23} If appropriate protocols are followed, the purity of the exchanged NCs is such that it is possible to remove even the last few residual cations from the initial “host lattice” that might be present in the final NCs.²² Also, depending on the miscibility of the reactant and of the product phases, partial replacement of the original cations

(which is feasible using substoichiometric amounts of the entering cations or, if possible, by arresting the exchange before completion) can be a tool for creating new types of heterostructures or alloyed NCs.^{2,10,12,21,24,25} For example, if the entering cations can coexist in the anion sublattice with the original ones, partial cation exchange represents a valid route for doping NCs or for creating alloyed NCs in order to tune and/or enhance their optical properties.^{23,26–28} An additional peculiar feature of cation exchange reactions is the possibility to access compositions and crystal structures that are metastable in the bulk or that do not exist in their bulk counterpart.^{10,17} Finally, new exciting directions are represented by the possibility to synthesize NCs of III–V semiconductors with this strategy.²⁹

In this work we report a systematic study involving tin ions (either Sn^{2+} or Sn^{4+}) as entering cations, and NCs of cubic berzelianite Cu_{2-x}Se NCs as the “host lattice”. Unlike previously reported exchange reactions, in which only one oxidation state of the entering cations was tested, the possibility for Sn to have two stable oxidation states (+2 and +4) can be exploited to investigate the combined effect of various valency related parameters (such as ionic radius, ionic charge, and type of

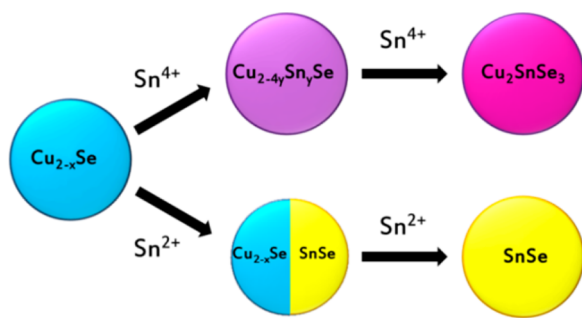
Received: August 8, 2014

Published: October 23, 2014

coordination to anions in the lattice) on the fate of a cation exchange reaction. In addition, Cu_{2-x}Se NCs possess features that make them an ideal “host lattice”: first, they remain stable in the cubic berzelianite phase through a wide range of Cu stoichiometries (in practice from values close to Cu_2Se to values close to $\text{Cu}_{1.75}\text{Se}$), with the only appreciable change represented by a small variation in the lattice parameters. This exemplifies enormously the structural analysis and makes the outcome of various experiments practically independent of the exact stoichiometry of the starting Cu_{2-x}Se NCs, which can vary slightly from synthesis to synthesis, and it is additionally related to cleaning, processing, and storing conditions of the NCs. Second, the ability of Cu_{2-x}Se NCs to easily exchange Cu^+ cations with a wide range of other cations makes it possible to investigate such exchange reactions under mild conditions.

In our experiments, when Sn^{4+} cations were used (Scheme 1 top), $\text{Cu}_{0.66}\text{Sn}_{0.33}\text{Se}$ NCs were formed, with intermediate steps

Scheme 1. Cation Exchange Reactions in Cu_{2-x}Se NCs Involving Sn^{4+} and Sn^{2+} Ions



being homogeneous alloyed NCs with roughly $\text{Cu}_{2-4y}\text{Sn}_y\text{Se}$ ($y \leq 0.33$) composition. Size and shape of the starting NCs were basically preserved, as well as the anion framework. The reaction stopped when the $\text{Cu}_{0.66}\text{Sn}_{0.33}\text{Se}$ (that is, Cu_2SnSe_3) stoichiometry was reached. These results are in line with a recent study by our group, in which we proved that, in metastable hexagonal $\text{Cu}_{2-x}\text{Se}_y\text{S}_{1-y}$ NCs, the Cu^+ cations could be exchanged with Sn^{4+} cations to form alloyed Cu–Sn–S systems while retaining the anionic sublattice.³⁰ Overall, this transformation can be explained by considering the following points: (i) Sn^{4+} ions have a size that is slightly smaller than that of the Cu^+ ions. This allows a gradual replacement of Cu^+ with Sn^{4+} ions throughout the NC lattice, with little influence on the anion framework, apart from a minor contraction to accommodate for the smaller Sn^{4+} ions. (ii) Once a $\text{Cu}_{0.66}\text{Sn}_{0.33}\text{Se}$ (that is Cu_2SnSe_3) composition is reached, cation exchange cannot proceed further, as this would require a drastic reorganization of the anion framework, which is apparently not possible at the mild reaction conditions under which the replacement is carried out. Higher reaction temperatures, on the other hand, cause reduction of the Sn^{4+} cations to Sn^{2+} in our experiments.

When instead Sn^{2+} ions were introduced (see Scheme 1 bottom), the starting Cu_{2-x}Se NCs were transformed to orthorhombic SnSe NCs, again with size and shape preservation, while the anion framework suffered a sensible reorganization. Differently from the Sn^{4+} case, in this reaction the intermediate steps were represented by $\text{Cu}_{2-x}\text{Se}/\text{SnSe}$ heterostructures. In this case, since Sn^{2+} ions are much larger than Cu^+ ions, when Sn^{2+} ions enter the lattice, they apparently

cannot coexist with Cu^+ ions in the cation sites and preserve at the same time the anion framework. This is also confirmed by the evidence that Cu_2Se and SnSe phases are immiscible in the bulk.³¹ The mild temperature at which we performed this Cu^+ to Sn^{2+} exchange (100 °C) suggests that the energetic barrier for the reorganization of the anion sublattice (going from a cubic to an orthorhombic symmetry) is relatively low.

EXPERIMENTAL SECTION

Chemicals. Oleylamine (Olam, 70%), oleic acid (OAc, 90%), 1-octadecene (ODE, 90%), 1-dodecanethiol (DDT, $\geq 98\%$), tin(II) chloride (SnCl_2 , 98%), tin(IV) bis(acetylacetonate) dichloride (SnAc_2Cl_2 , 98%), and tetrachloroethylene anhydrous (TCE, $\geq 99\%$) were purchased from Sigma-Aldrich. Copper(I) chloride (CuCl , 99.999%), selenium powder (Se, 99.99%), and tri-n-octylphosphine (TOP, min. 97%) were purchased from Strem Chemicals. Anhydrous methanol, toluene, and isopropanol were purchased from Carlo Erba. All chemicals were used without further purification.

Synthesis of Cu_{2-x}Se Nanocrystals. The synthesis of Cu_{2-x}Se nanocrystals was carried out following our previous work:³² 1 mmol of CuCl was first dissolved in 2 mL of degassed Olam in a N_2 filled glovebox at 160 °C for 1 h. At the same time a mixture of Olam (3 mL) and ODE (5 mL) was degassed under vacuum in a reaction flask at 120 °C for 2 h, using a standard Schlenk line. The CuCl/Olam solution was then transferred into the reaction flask that had been previously put under nitrogen flux. The temperature was set to 310 °C. A solution of Se in Olam (prepared by mixing 0.5 mmol of Se powder with 3 mL of Olam and kept at 100 °C) was rapidly hot injected into the reaction flask at 280 °C. After the injection, the temperature of the reaction was allowed to reach 310 °C. The overall reaction time after the injection was 15 min, after which the flask was rapidly cooled to room temperature. This crude reaction solution was immediately used for the cation exchange reactions following *in situ* approaches (see later). Alternatively, the NCs were dissolved in 5 mL of toluene and precipitated with the addition of 15 mL of methanol. After this washing step, the Cu_{2-x}Se NCs were dissolved in toluene. The yield of the Cu_{2-x}Se NCs synthesis was determined by ICP elemental analysis as $\sim 55\%$ (i.e., 0.55 mmol of Cu^+ is contained inside the Cu_{2-x}Se NCs synthesized in the reaction flask).

Exchange Reactions Involving Sn^{4+} Ions. We developed an *in situ* approach to exchange Cu^+ ions with Sn^{4+} ions. After quenching the Cu_{2-x}Se NC synthesis the crude reaction mixture was heated to 100 °C. At this point a solution of SnAc_2Cl_2 in ODE (4 mL) and DDT (1 mL), prepared in the glovebox at 130 °C, was transferred into the reaction flask together with 2 mL of TOP. After the injection the temperature of the reaction was allowed to reach 100 °C for 10 min (see Table 1 for details). The NCs were then washed twice by precipitation with addition of methanol followed by redissolution in toluene. At each cleaning step a small amount of Olam (50 μL) was added in order to stabilize the colloidal suspension. The $\text{Cu}_{2-4y}\text{Sn}_y\text{Se}$ NCs were eventually dispersed in toluene and stored in the glovebox.

Table 1. Synthetic Parameters of the Different Cation Exchange Procedures with the Corresponding Products

cation	synthesis	Sn/Cu molar ratio	T	time (min)	product ^a
Sn^{4+}	<i>in situ</i>	0.4/0.55	100 °C	10	$\text{Cu}_{0.66}\text{Sn}_{0.33}\text{Se}$
	<i>in situ</i>	0.1/0.55	100 °C	10	$\text{Cu}_{1.20}\text{Sn}_{0.19}\text{Se}$
	<i>in situ</i>	0.05/0.55	100 °C	10	$\text{Cu}_{1.85}\text{Sn}_{0.07}\text{Se}$
Sn^{2+}	two pot	0.125/0.25	100 °C	1	SnSe
	two pot	0.04/0.15	100 °C	1	$\text{Cu}_{2-x}\text{Se}/\text{SnSe}$
	<i>in situ</i>	1.5/0.55	100 °C	1	$\text{SnSe} + \text{Cu}_{2-4y}\text{Sn}_y\text{Se}$

^aThe stoichiometry of the products was calculated via inductively coupled plasma (ICP) elemental analysis and confirmed by energy dispersive X-ray spectroscopy (EDS).

Exchange Reactions Involving Sn^{2+} Ions. In a typical cation exchange reaction with Sn^{2+} ions, a solution of SnCl_2 in Olam (2 mL) and ODE (3 mL) was degassed under vacuum in a reaction flask at 100 °C for 2 h. At this point a mixture of TOP (2 mL) and Cu_{2-x}Se NCs in toluene was added to the reaction flask, and the solution was allowed to react for 1 min at 100 °C (see Table 1 for details). The crystals were washed two times by dissolution in toluene followed by precipitation upon addition of methanol. At each cleaning step a small amount of OAc (50 μL) was added in order to stabilize the colloidal suspension. The SnSe NCs were eventually dispersed in toluene and stored in a glovebox.

An *in situ* approach was additionally investigated in the $\text{Cu}^+ \rightarrow \text{Sn}^{2+}$ exchange reaction. In this case, after quenching the Cu_{2-x}Se NC synthesis, the crude reaction mixture was heated to 100 °C. A solution of SnCl_2 in ODE (3 mL) and Olam (2 mL), prepared in glovebox at 100 °C, was then transferred into the reaction flask together with 2 mL of TOP. After the injection the temperature of the reaction was allowed to reach 100 °C for 1 min (see Table 1 for details). The crystals were washed two times by precipitation with addition of methanol followed by redissolution in toluene. At each cleaning step a small amount of OAc (50 μL) was added in order to stabilize the colloidal suspension. The resulting NCs were eventually dispersed in toluene and stored in a glovebox.

Structural Characterization and Elemental Analysis. TEM Measurements. The samples were prepared by dropping dilute solutions of NCs onto carbon coated gold grids and placed in a pumping station in order to let the solvent evaporate completely and preserve them from oxidation. Low-resolution transmission electron microscopy (TEM) measurements were carried out on a JEOL-1100 transmission electron microscope operating at an acceleration voltage of 100 kV. High resolution TEM (HRTEM) was performed with a JEOL JEM-2200FS microscope equipped with a field emission gun working at an accelerating voltage of 200 kV, a CEOS spherical aberration corrector of the objective lens, which enables a spatial resolution of 0.9 Å, and an in column Omega filter. The chemical composition of the NCs was determined by energy dispersive X-ray spectroscopy (EDS) analysis performed in high angle annular dark field scanning TEM (HAADF-STEM) mode with a Bruker Quantax 400 system with a 60 mm² XFlash 6T silicon drift detector (SDD), using the Cliff–Lorimer method.

X-ray Diffraction (XRD) Measurements. XRD measurements were performed on a Rigaku SmartLab X-ray diffractometer operating at 40 kV and 150 mA. The diffractometer was equipped with a Cu source and a Gobel mirror in order to have a parallel beam, and it was used in $2\theta/\omega$ scan geometry for the acquisition of the data. Specimens for the XRD measurements were prepared in the glovebox by dropping a concentrated NCs solution onto a zero-background silicon substrate.

Elemental Analysis. This was carried out via inductively coupled plasma atomic emission spectroscopy (ICP-AES), using a iCAP 6500 Thermo spectrometer. Samples were dissolved in HCl/HNO₃ 3:1 (v/v). All chemical analyses performed by ICP-AES were affected by a systematic error of about 5%.

Optical Spectroscopy. Raman Analysis. The pristine NCs were dropcast on silicon substrates under inert atmosphere. Raman spectra of $\text{Cu}_{2-4y}\text{Sn}_y\text{Se}$ NCs were performed under air with a Jobin Yvon HR800 spectrometer at an excitation wavelength of 632.8 nm. The laser source (nominal power 0.5 mW) was focused on the sample through a 100 \times objective, with an integration time of 120 s. In the case of SnSe and $\text{Cu}_{2-x}\text{Se}/\text{SnSe}$ NCs the measurements were performed under inert atmosphere in order to avoid oxidation phenomena.³³ For this purpose, nitrogen was fluxed through a closed chamber (from Linkam) coupled with a Renishaw InVia spectrometer. Data were acquired at $\lambda = 632.8$ nm with a 50 \times objective using a nominal power of 25 mW and an integration time of 30 s.

UV–Vis–NIR Absorption. The copper and tin based NCs dispersed in toluene were dried under nitrogen flux to remove the solvent and were redispersed in anhydrous TCE to perform the measurements. The UV–vis–NIR absorption spectra of the NCs solutions were recorded using a Varian Cary 5000 UV–vis–NIR absorption spectrophotometer.

RESULTS AND DISCUSSION

In copper chalcogenide NCs, exchange reactions from Cu^+ to M^{n+} ions are facilitated by the acid softness of Cu^+ cations ($\eta = 6.3$ eV³⁴) that can be easily solvated by a soft base like tri-n-octylphosphine ($\eta \sim 6$ eV⁹). This, in turn, favors the entrance of multivalent M^{n+} cations in the NC lattice.¹⁴ In our sets of experiments, the starting Cu_{2-x}Se NCs were reacted either with Sn^{2+} or with Sn^{4+} cations at relatively low temperature, namely 100 °C. Sn ions, depending on their oxidation state, have a radius that can be considerably larger ($\text{Sn}^{2+} \sim 118$ pm) or comparable ($\text{Sn}^{4+} \sim 55\text{--}81$ pm) to that of the Cu^+ cations ($\sim 60\text{--}77$ pm).³⁵ In the case of the small Sn^{4+} ions, it is likely that exchange reactions are mediated by both diffusion of Cu vacancies and interstitial diffusion of the Sn^{4+} ions in the NC lattice, while for the larger Sn^{2+} ions interstitial diffusion should be hindered (see later). While the presence of TOP was mandatory for the cation exchange reactions to take place, the choice of specific reaction conditions, for example the use of DDT and Olam coupled with Sn^{4+} and Sn^{2+} ions, respectively, was dictated primarily by the need to prepare stable solutions of the cations (i.e., solutions in which the cations were soluble and did not undergo redox reactions at our experimental conditions).

We will discuss first the results on the cation exchange reactions involving Sn^{4+} ions. Figure 1a,b shows typical TEM images of the initial Cu_{2-x}Se NCs and of the corresponding NCs with $\text{Cu}_{0.66}\text{Sn}_{0.33}\text{Se}$ (or Cu_2SnSe_3) stoichiometry, that is, with the highest possible content in Sn (determined by both EDS and ICP analysis) that could be reached by the $\text{Cu}^+ \rightarrow$

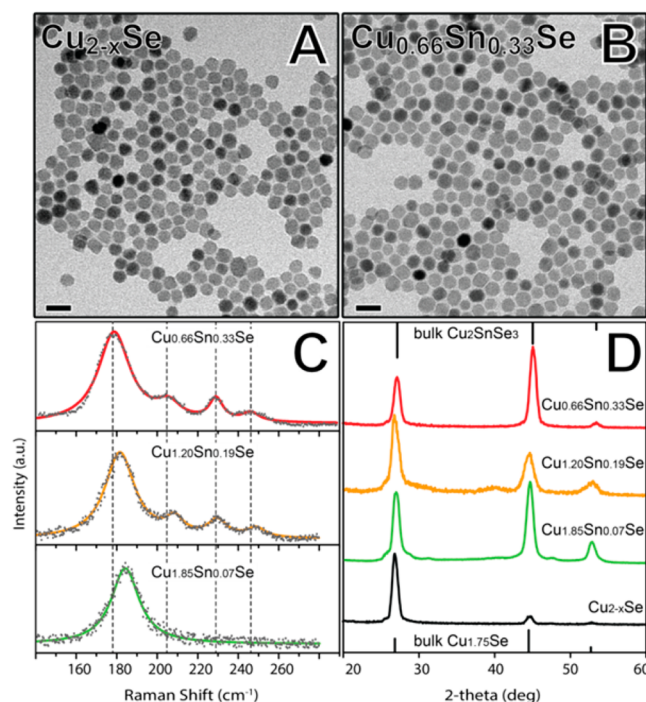


Figure 1. Low resolution TEM images of (a) pristine Cu_{2-x}Se and (b) $\text{Cu}_{0.66}\text{Sn}_{0.33}\text{Se}$ (or Cu_2SnSe_3) NCs. The scale bars in both figures are 20 nm. (c) Raman spectra of different $\text{Cu}_{2-4y}\text{Sn}_y\text{Se}$ samples. (d) X-ray diffraction patterns obtained from dropcast solutions of Cu_{2-x}Se and different $\text{Cu}_{2-4y}\text{Sn}_y\text{Se}$ NCs. The corresponding bulk reflections of $\text{Cu}_{1.75}\text{Se}$ (ICDD 01-075-2714) and Cu_2SnSe_3 (ICDD 03-065-4145) are reported. The stoichiometry of the samples was determined by ICP elemental analysis.

Sn^{4+} exchange route. The images suggest that size and morphology of the NCs are both preserved in this process, as the size of the final $\text{Cu}_{0.66}\text{Sn}_{0.33}\text{Se}$ NCs and of the starting Cu_{2-x}Se NCs measured from the TEM images are, respectively, 11.4 ± 1.6 and 11.9 ± 2.8 nm. The corresponding size distribution histograms are presented in Figure S1 of the Supporting Information (SI). We could also prepare NCs with compositions that were intermediate between the starting Cu_{2-x}Se NCs and the $\text{Cu}_{0.66}\text{Sn}_{0.33}\text{Se}$ ones, as confirmed by elemental analysis. The XRD patterns of the various samples (initial, final, and two intermediates) are reported in Figure 1d. The patterns indicate that, by increasing the amount of Sn^{4+} cations incorporated within the Cu_{2-x}Se NCs, the crystal lattice gradually evolves to that of the cubic Cu_2SnSe_3 structure.

X-ray diffraction, however, is not the most suitable tool for monitoring such transformation, due to the small difference in lattice parameters between Cu_{2-x}Se and Cu_2SnSe_3 . A more appropriate tool is instead Raman spectroscopy: as reported in Figure 1c, a gradual evolution was also seen in the Raman spectra collected from the very same samples. The pristine Cu_{2-x}Se NCs did not exhibit any Raman features, and therefore, the spectrum is not shown. This is most likely due to the very low Raman scattering efficiency of this phase, as already observed recently by Izquierdo-Roca et al.³⁶ Starting from the pristine Cu_{2-x}Se NCs, already at the very early stages of the $\text{Cu}^+ \rightarrow \text{Sn}^{4+}$ exchange (for example when the composition was $\text{Cu}_{1.85}\text{Sn}_{0.07}\text{Se}$, as measured by elemental analysis via ICP) a broad peak at about 185 cm^{-1} was observed (see Figure 1c). This peak appears to be related to the main mode of the $\text{Cu}_{0.66}\text{Sn}_{0.33}\text{Se}$ phase,^{37,38} albeit blue-shifted by few cm^{-1} from that mode. Upon increasing the amount of Sn^{4+} ions incorporated in the Cu_{2-x}Se NCs (for example at a composition corresponding to $\text{Cu}_{1.20}\text{Sn}_{0.19}\text{Se}$), all peaks traceable to the Raman modes of the Cu_2SnSe_3 phase were observed, although almost all of them were slightly blue-shifted from those modes. The final $\text{Cu}_{0.66}\text{Sn}_{0.33}\text{Se}$ NCs exhibited a main peak at 179 cm^{-1} and three minor peaks at 205, 228, and 245 cm^{-1} , in good agreement with literature data for the Cu_2SnSe_3 phase.^{37,38} The appearance and the progressive shift of the $\text{Cu}_{0.66}\text{Sn}_{0.33}\text{Se}$ Raman modes that followed the entrance of Sn^{4+} ions inside the Cu_{2-x}Se NCs support the formation of solid $\text{Cu}_{2-4y}\text{Sn}_y\text{Se}$ solutions as intermediate phases.

While the gradual replacement of copper with tin was corroborated by elemental analysis via ICP (see Table 1), the formation of alloyed structures instead of heterostructures was additionally confirmed by EDS analysis of individual NCs, which indicated an homogeneous distribution of Sn in each NC. This is reported in Figure S3 of the Supporting Information. Similarly, HRTEM analysis (see Figure 2) indicated that the replacement of Cu^+ by Sn^{4+} ions led to the formation of alloyed NCs: in going from Cu_{2-x}Se NCs to $\text{Cu}_{0.66}\text{Sn}_{0.33}\text{Se}$ NCs only monocrystalline particles were observed, with a small and gradual contraction in lattice parameters, from values typical of Cu_{2-x}Se , to those of $\text{Cu}_{0.66}\text{Sn}_{0.33}\text{Se}$. This variation followed the progressive substitution of Cu^+ with Sn^{4+} cations and confirmed that the cation exchange resulted in the formation of alloyed Cu–Sn–Se NCs.

The berzelianite Cu_{2-x}Se phase (ICSD card no. 59956) and the cubic $\text{Cu}_{0.66}\text{Sn}_{0.33}\text{Se}$ (or Cu_2SnSe_3) phase (ICSD card no. 103097) lattices are characterized by an isostructural fcc anionic sublattice, with four formula units per unit cell ($Z = 4$), and similar lattice parameters, namely 5.776 Å in berzelianite and 5.696 Å in Cu_2SnSe_3 . The difference in unit cell volumes

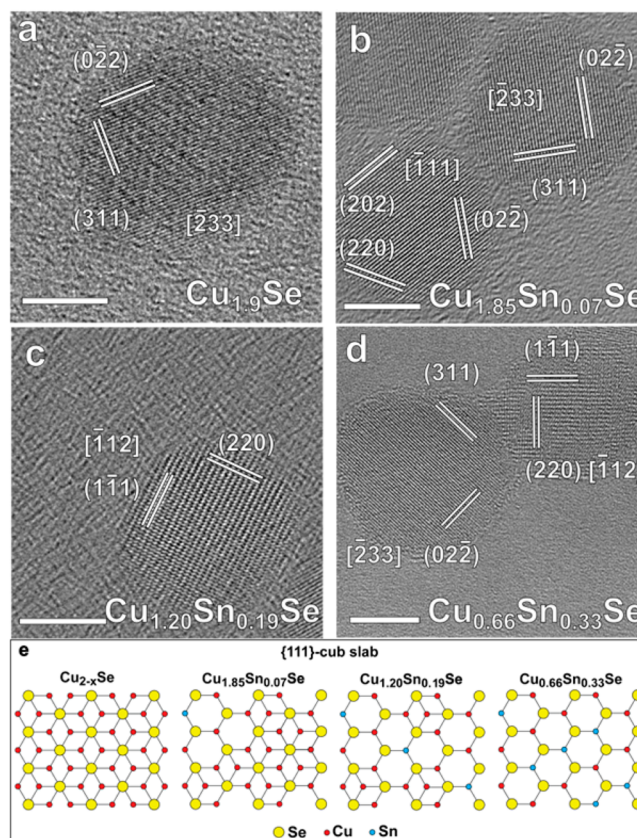


Figure 2. HRTEM imaging of a series of cation exchanged NCs using Sn^{4+} . (a) Parent Cu_{2-x}Se . (b) Intermediate $\text{Cu}_{1.85}\text{Sn}_{0.07}\text{Se}$. (c) Intermediate $\text{Cu}_{1.20}\text{Sn}_{0.19}\text{Se}$. (d) Final $\text{Cu}_{0.66}\text{Sn}_{0.33}\text{Se}$. The images sketch the typical lattice sets of fcc lattice. The scale bars in the figures are 5 nm. (e) Atomic schema representing {111} lattice slabs of Cu_{2-x}Se , $\text{Cu}_{1.85}\text{Sn}_{0.07}\text{Se}$, $\text{Cu}_{1.20}\text{Sn}_{0.19}\text{Se}$, and $\text{Cu}_{0.66}\text{Sn}_{0.33}\text{Se}$ showing their structural isomorphism.

between the two phases is only 4%. In both Cu_{2-x}Se and cubic $\text{Cu}_{0.66}\text{Sn}_{0.33}\text{Se}$ the anion sublattice, made of Se atoms arranged in cubic close packing, forms the same polyhedral cation sites, resulting then in four possible exchangeable tetrahedral sites at (0.25; 0.25; 0.25) for every $1 \times 1 \times 1$ unit cell and considering the origin of the isometric basis vectors on a generic Se atom. Cu_{2-x}Se and $\text{Cu}_{0.66}\text{Sn}_{0.33}\text{Se}$ crystals are then characterized by a different status of cation occupancy within the (0.25; 0.25; 0.25) sites, i.e., single (only Cu^+) in berzelianite and mixed ($\text{Cu}^+ + \text{Sn}^{4+}$) in copper tin selenide. Some structural considerations have to be taken into account in order to explain the effects following the cation exchange reaction from Cu_{2-x}Se to $\text{Cu}_{0.66}\text{Sn}_{0.33}\text{Se}$ NCs. In berzelianite Cu_{2-x}Se two copper sites are present: Cu1 sites with tetrahedral coordination at (0.25; 0.25; 0.25) with multiplicity 8 and nontetrahedral Cu2 sites at (0.3333; 0.3333; 0.3333) with multiplicity 32. Both sites are characterized by a partial occupancy in Cu, which is 0.8 for Cu1 and 0.03 for Cu2 sites, respectively. Cubic $\text{Cu}_{0.66}\text{Sn}_{0.33}\text{Se}$ contains, conversely, a single type of cation site at (0.25; 0.25; 0.25) with tetrahedral coordination and multiplicity 4, characterized by a mixed occupancy, 0.67 in Cu^+ and 0.33 in Sn^{4+} (see Figure S2 and the structural paragraph of the Supporting Information for details). By comparing these two phases (Cu_{2-x}Se and $\text{Cu}_{0.66}\text{Sn}_{0.33}\text{Se}$) we can deduce that, upon cation exchange from the pristine Cu_{2-x}Se NCs to the final $\text{Cu}_{0.66}\text{Sn}_{0.33}\text{Se}$ NCs, the following

changes must take place: (i) There is partial replacement of Cu^+ ions in the tetrahedral Cu1 (0.25; 0.25; 0.25) sites with Sn^{4+} ions diffusing there. Consequently, the Cu occupancy in the Cu1 sites drops from 0.8 of Cu_{2-x}Se to 0.67 of $\text{Cu}_{0.66}\text{Sn}_{0.33}\text{Se}$. (ii) There is total emptying of the non-tetrahedral Cu2 sites at (0.333; 0.333; 0.333). (iii) There is small cell shrinkage due to replacement of Cu^+ ions (0.6 Å radius) with smaller Sn^{4+} ions (0.55 Å radius) and partial Cu^+ depletion.

The results from our experiments indicate that when Sn^{4+} ions were reacted with Cu_{2-x}Se NCs, there was a gradual replacement of Cu^+ with Sn^{4+} ions throughout the NC lattice that led to the formation of alloyed $\text{Cu}_{2-4y}\text{Sn}_y\text{Se}$ NCs with y being 0.33 at maximum, similarly to what we recently observed using hexagonal $\text{Cu}_{2-x}\text{Se}_y\text{S}_{1-y}$ nanoplatelets as starting seeds.³⁰ Given the small size of the cations involved (both Cu^+ and Sn^{4+}), most likely this exchange reaction is mediated by both diffusion of Cu vacancies (abundant in the Cu_{2-x}Se NCs) and by interstitial diffusion of the Sn^{4+} ions. Both processes appear to be fast and isotropic in the present case as we do not see the formation of segmented heterostructures nor of core/shell ones. The only apparent requirement here was that of charge balance; i.e., each Sn^{4+} ion introduced had to be matched by the departure of 4 Cu^+ ions. Interestingly, the intermediate cubic $\text{Cu}_{2-4y}\text{Sn}_y\text{Se}$ alloyed structures that we found here could not be predicted by the bulk Cu_2Se – SnSe_2 phase diagram,³¹ and only in a recent work by Fan et al. was a stable $\text{Cu}_5\text{Sn}_2\text{Se}_7$ compound, that is, with $\text{Cu}_{0.71}\text{Sn}_{0.29}\text{Se}$ stoichiometry, reported for the first time.³⁹ On the other hand, the replacement of Cu^+ with Sn^{4+} cations could not go beyond the Cu_2SnSe_3 stoichiometry. Such experimental evidence can be easily rationalized by looking at the end, stable structure that would result from a complete replacement of Cu^+ with Sn^{4+} cations, that is, trigonal SnSe_2 . This is a layered material characterized by a stack of SnSe_2 layers bound together by weak Se–Se van der Waals bonds, i.e., much different from the initial structure having a fcc anion sublattice.⁴⁰ A complete cation exchange in this case would entail a pervasive reorganization of the anion framework requiring energies that are not accessible at the low temperature at which the cation exchange experiments are carried out (i.e., 100 °C). No SnSe_2 phase was indeed observed in our experiments. Furthermore, attempts to carry out such $\text{Cu}^+/\text{Sn}^{4+}$ exchange at higher temperature (200 °C for example) resulted in the formation of SnSe NCs accompanied by morphological changes in the particles (see Figure S7 of Supporting Information and the corresponding paragraph for details). Under these conditions, the Sn^{4+} ions were reduced (most likely by the alkyl thiol present in solution) to Sn^{2+} before they could react with the particles.

We now discuss the results related to the exchange of Cu^+ ions with Sn^{2+} ions, with a caution for the reader that in this case an *ex situ* (or two pot) reaction scheme was adopted, as described in detail in the Experimental Section. This is due to the fact that if the Sn^{2+} cations were directly injected into the Cu_{2-x}Se NC reaction flask at 100 °C, as was done for the previous experiments, we had strong indications that part of the Sn^{2+} ions were oxidized to Sn^{4+} , which complicated the interpretation of the data (see Table 1 and Figure S6 of the Supporting Information). It is likely that the oxidation of Sn^{2+} to Sn^{4+} was operated by the excess of unreacted Cu^+ ions still present in the reaction flask. If one considers indeed the reduction potentials of the species involved in the reaction, the only spontaneous redox reaction would be $\text{Sn}^{2+} + 2\text{Cu}^+ \rightarrow \text{Sn}^{4+}$

+ 2Cu^0 while the disproportionation of Sn^{2+} and the reduction of Se^0 to Se^{2-} are hindered at our synthetic conditions. With this caution in mind, elemental analysis via ICP (Table 1) indicated that in the two pot approach a complete exchange of copper with tin was possible and that the final stoichiometry was SnSe . The TEM images shown in Figure 3a,b suggest that

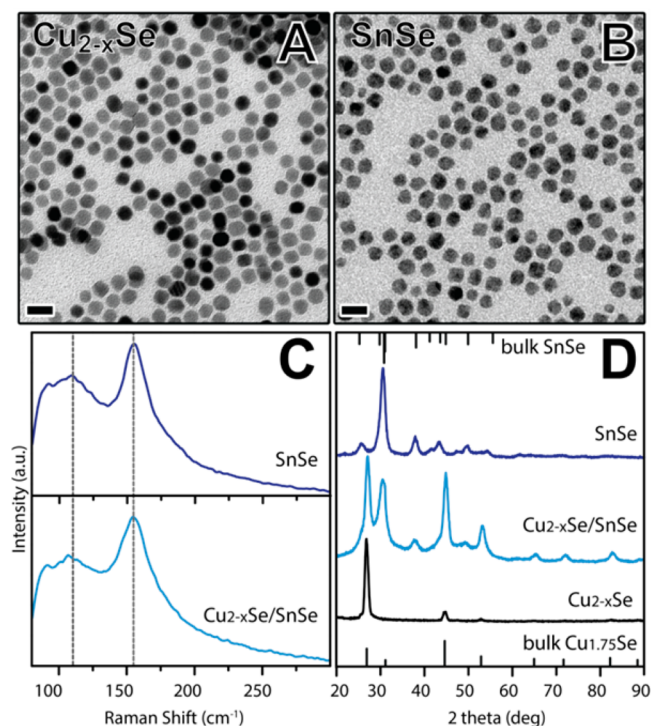


Figure 3. Low resolution TEM images of (a) pristine Cu_{2-x}Se and (b) SnSe NCs. The scale bars in both figures are 20 nm. (c) Raman spectra of SnSe and $\text{Cu}_{2-x}\text{Se}/\text{SnSe}$ samples. (d) X-ray diffraction patterns obtained from dropcast solutions of Cu_{2-x}Se , SnSe NCs, and $\text{Cu}_{2-x}\text{Se}/\text{SnSe}$ heterostructures. The corresponding bulk reflections of $\text{Cu}_{1.75}\text{Se}$ (ICDD 01-075-2714) and SnSe (ICDD 01-089-0233) are reported.

the size of the NCs is preserved in this process too, although slight changes in the morphologies of the NCs cannot be excluded. The average size of the final SnSe NCs was equal to 11.9 ± 1.9 nm, indeed very close to that of the initial Cu_{2-x}Se NCs (the corresponding size distribution histograms are presented in Figure S1, Supporting Information).

According to the XRD analysis (Figure 3d, top plot), the Cu_{2-x}Se NCs were transformed into orthorhombic SnSe NCs. Also in this transformation we could achieve a partial replacement of copper with tin, as evidenced by ICP analysis (Table 1), when using a substoichiometric amount of Sn^{2+} . A typical XRD pattern of a partially exchanged sample is reported in Figure 3d, middle plot. The pattern contains both peaks of the starting cubic Cu_{2-x}Se NC sample (Figure 3d, bottom plot) and of orthorhombic SnSe (top plot), suggesting that the sample is a mixture of Cu_{2-x}Se and SnSe phases. This is supported also by Raman analysis. As we know from the previous discussion, the Cu_{2-x}Se NCs did not exhibit any noticeable Raman peak. On the other hand, the partially exchanged sample (Figure 3c, bottom plot) exhibited two main peaks at 110 and 155 cm^{-1} that are characteristic of orthorhombic SnSe .⁴¹ No additional peaks, which could be ascribed to other phases (i.e., Cu–Sn–Se alloys at 180 cm^{-1}),

were present. The position of these peaks did not change in the sample that was completely exchanged (Figure 3c, top plot). Overall, these results indicate that even partial replacement of Cu^+ with Sn^{2+} leads to the formation of SnSe right from the beginning, and that no other compounds (for example alloys) are present, except for residual Cu_{2-x}Se .

The comparison of XRD peaks from the Cu_{2-x}Se phase in the pristine sample and in the partially exchange sample (Figure 3d) is noteworthy. In the pristine sample, the intensity ratio of the (111)/(220) reflections from Cu_{2-x}Se (at roughly 27° and 45° , respectively) is much higher than that from the bulk $\text{Cu}_{1.75}\text{Se}$ pattern. This is mainly due to a preferential orientation of the Cu_{2-x}Se NCs in the film (see Figure S8 and Supporting Information for further experiments on films of Cu_{2-x}Se NCs supporting this claim). In the partially exchanged sample, the (111)/(220) ratio is instead closer to the one expected for a bulk powder, which indicates a substantial lack of preferential orientation of the Cu_{2-x}Se NCs in this case. A similar loss of preferential orientation in films of NCs is observed in the XRD patterns of $\text{Cu}_{2-y}\text{Sn}_y\text{Se}$ alloy NCs of Figure 1d, and it can be due to reorganization of the ligand shell around the NCs following cation exchange, which might not allow the NCs to stack into locally ordered structures. The inability of the NCs to locally order might also be due to a slight reshaping of the NCs, especially in the $\text{Cu}_{2-x}\text{Se}/\text{SnSe}$ case.

As observed by HRTEM, the fully exchanged sample was indeed mostly composed of monocrystalline orthorhombic SnSe NCs, as shown in Figure 4a, with a small minority of cubic and polycrystalline SnSe NCs (see also Figure S5 of the Supporting Information and the discussion below). The small minority of cubic SnSe nanocrystals might be ascribed to a

direct transition of a few Cu_{2-x}Se NCs into metastable cubic SnSe via cation exchange, with retention of the Se sublattice of the pristine Cu_{2-x}Se phase. On the other hand, the partially exchanged sample was composed of a mixture of completely exchanged NCs (i.e., SnSe), pristine (that is, not yet exchanged) Cu_{2-x}Se NCs, and many $\text{Cu}_{2-x}\text{Se}/\text{SnSe}$ heterostructures. The latter were characterized by clean interfaces between the two different domains, such as in the NC shown in Figure 4b.

The formation of heterostructures is similar to what was observed in previous works on cation exchange reactions between CdS NCs and Cu^+ and Ag^+ ions.^{21,24} In most of the heterostructures, the SnSe domain was a single crystal domain that most likely was formed when cation exchange occurred at a single front within a NC. In that case, the resulting heterostructure showed imperfect epitaxial relationships, due to the distortion of the anionic sublattice by the introduction of Sn^{2+} ions (see Figure S4 and the related paragraph of the Supporting Information for details). In other heterostructures, the exchanged portions consisted of multiple SnSe domains (see figure S5 of the Supporting Information). In those cases, it is likely instead that cation exchange had occurred through multiple fronts in a given Cu_{2-x}Se NC, leading eventually to the polycrystalline SnSe NCs observed in HRTEM (see Supporting Information Figure S5).

In the $\text{Cu}^+ \rightarrow \text{Sn}^{2+}$ exchange reaction, different from the $\text{Cu}^+ \rightarrow \text{Sn}^{4+}$ case discussed earlier, the preservation of the anionic sublattice is not assured anymore. This is best exemplified in the sketches of Figure 4c. The orthorhombic SnSe phase (ICSD card no. 186650, space group $Pnma$), with lattice parameters $a = 11.75 \text{ \AA}$, $b = 4.154 \text{ \AA}$, $c = 4.446 \text{ \AA}$, can be seen as a distorted NaCl cubic structure⁴² with a doubling of a lattice parameter. From a structural point of view, the SnSe {201} lattice planes of orthorhombic basis vectors $\{\mathbf{a}, \mathbf{b}, \mathbf{c}\}$ display a distorted cubic-close-packing of Se atoms that can be also interpreted as {111} lattice planes of a pseudocubic subcell with the new basis vector $\{\mathbf{a}', \mathbf{b}', \mathbf{c}'\}$, after the application of a transformation matrix. Consequently, the orthorhombic basis vector of SnSe can also be described according to a pseudo cubic subcell by applying the transformation matrix $(\frac{1}{2}00)/(\frac{0^+}{2}\frac{1}{2})/(\frac{0^+}{2}\frac{1}{2})$, where the $[200]/[0\bar{1}1]/[011]$ vectors of SnSe are the basis vector of the new pseudocubic unit cell:

$$\mathbf{a}' = \frac{1}{2}\mathbf{xa}; \quad \mathbf{b}' = -\mathbf{xb} + \mathbf{xc}; \quad \mathbf{c}' = \mathbf{xb} + \mathbf{xc}$$

with $\mathbf{a}' = 5.75 \text{ \AA}$, $\mathbf{b}' = 6.08 \text{ \AA}$, $\mathbf{c}' = 6.08 \text{ \AA}$ and $\alpha' = 86.05^\circ$, $\beta' = 90^\circ$, $\gamma' = 90^\circ$.

With such geometrical considerations in mind, we can now summarize the steps involved in the $\text{Cu}^+ \rightarrow \text{Sn}^{2+}$ exchange reaction. First, since such reaction implies a total Cu depletion, all Cu^+ ions are removed from the Cu1 and Cu2 sites of pristine Cu_{2-x}Se NCs. The empty sites in the Se sublattice are filled by Sn^{2+} cations, which distort the cubic structure of Cu_{2-x}Se into the orthorhombic lattice of SnSe. In particular, the Se anion sublattice distortion of the parent Cu_{2-x}Se lattice, due to exchange with Sn^{2+} , will occur preferentially along the cubic close-packed direction {111}. This can be best depicted by looking at the cross-section of a {111} slab of Cu_2Se , where ordered couples of Se^{2-} ions are alternately shifted upward and downward along the vertical {111} axis (see lower sketches of Figure 4c).

The formation of the $\text{Cu}_{2-x}\text{Se}-\text{SnSe}$ heterostructures can be then explained by considering that berzelianite Cu_{2-x}Se is not

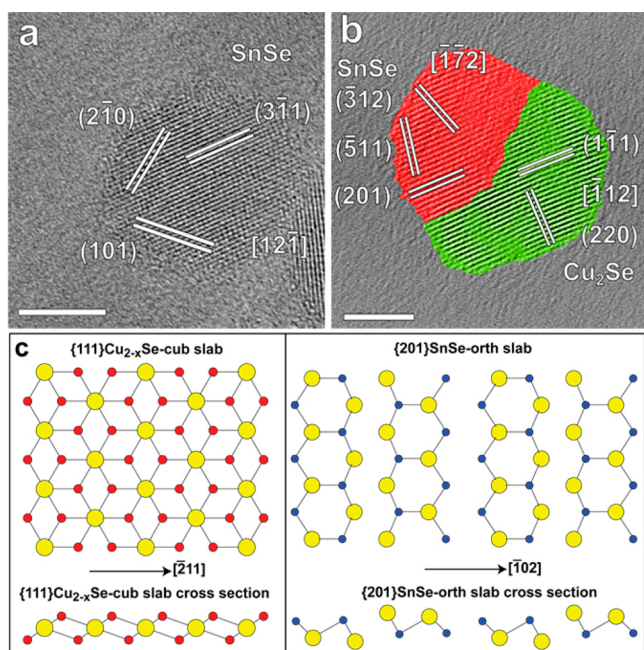


Figure 4. (a) HRTEM of a representative exchanged SnSe NC. (b) HRTEM image of a representative $\text{Cu}_{2-x}\text{Se}/\text{SnSe}$ heterostructure exhibiting the different domains (SnSe in red and Cu_{2-x}Se in green) separated by quasiepitaxial interfaces and showing the typical lattice sets of the corresponding cubic and orthorhombic crystal structures. Scale bars in all the HRTEM images are 5 nm. (c) Atomic schemas of cubic {111} Cu_{2-x}Se and orthorhombic {201} SnSe slabs showing the similarities between the two structures.

able to evolve to a ternary Cu–Sn–Se compound by accommodating large Sn^{2+} cations (1.18 Å radius) in the tetrahedrally coordinated (0.25; 0.25; 0.25) sites without causing a drastic distortion of the Se anionic sublattice and a significant change in symmetry. This is in accordance with the Cu_2Se – SnSe phase diagram,³¹ as the cubic Cu_{2-x}Se and the orthorhombic SnSe phases are known to be immiscible. Therefore, only distinct domains with SnSe composition are created, which coexist in the same NC with pristine, nonexchanged Cu_{2-x}Se domains when the replacement has not reached completion. On the other hand, with the difference in the lattice volume between the reactant and the product being around 7%, the stress developed in the NC lattice during the reaction is not enough to produce substantial morphological change of the NCs (see Figure 3a,b) as observed instead in cation exchange reactions of some metal chalcogenide NCs: $\text{CdE} \rightarrow \text{M}_x\text{E}_y$ ($\text{E} = \text{S, Se, Te}$; $\text{M} = \text{Pd, Pt}$).¹⁴

The formation of Janus-like $\text{Cu}_{2-x}\text{Se}/\text{SnSe}$ heterostructures rather than core–shell ones can be qualitatively explained by considering that, most likely, the large Sn^{2+} cations can enter the Cu_{2-x}Se NCs and replace Cu^+ ions only through a Cu vacancy diffusion-mediated mechanism and not additionally through interstitial diffusion of Sn^{2+} ions. As such, the replacement might not start until a threshold number of Cu vacancies is occasionally reached at one location at the surface of a NC. After that, the replacement will continue from there at a sustained rate in the NC. It is also true that the ligands bound to the surface of a NC might play a role in determining which specific site on the surface is preferred for the cation exchange to start on. However, we believe that the formation of heterostructures here is most likely a consequence of the fact that the Cu vacancies have to accumulate in a specific spot on the NC surface in order to allow the cation exchange process to take place. Such proposed mechanism would explain why in the partially exchanged sample we could observe, in addition to heterostructures, pristine (unexchanged) NCs as well as completely exchanged NCs. Furthermore, the presence of many polycrystalline SnSe NCs in the fully exchanged NCs can be rationalized by considering that, statistically, there could be instances in which the barrier to initiate cation exchange is almost simultaneously overcome in more than one location on the surface of a NC. In that case, cation exchange can occur through multiple fronts inside an individual NC.

The incorporation of Sn ions (either Sn^{2+} or Sn^{4+}) had a profound influence on the optical properties of the starting Cu_{2-x}Se NCs. As it is possible to notice from Figure 5, the incorporation of either Sn^{2+} or Sn^{4+} ions shifted the absorption onset of the initial NCs toward lower energies, indicating a narrowing of the optical bandgap. Moreover, the broad

absorption peak ranging from about 800 nm to the near-IR region of the Cu_{2-x}Se NCs (which is ascribed to a localized surface plasmon resonance mode, and arising from copper deficiency in copper chalcogenides^{32,43–48}) was basically suppressed after the exchange with tin cations (see Figure 5).

The disappearance of the plasmon peak of the Cu_{2-x}Se NCs when exposed to Sn^{4+} ions supported the formation of Cu–Sn–Se solid solutions even when working with very tiny amount of tin (see Figure 5a). This suggests that the incorporated Sn^{4+} ions, even in very small amounts, could be effective in filling the copper vacancies, or in trapping free charge carriers behaving as dopants, and so in suppressing the plasmon properties of the Cu_{2-x}Se NCs. In the exchange process with Sn^{2+} ions, no plasmon peak appeared, not even in the $\text{Cu}_{2-x}\text{Se}/\text{SnSe}$ heterostructures. This could be qualitatively explained by considering that, after a fraction of the Cu_{2-x}Se NCs had undergone exchange with Sn^{2+} ions, part of the extracted Cu^+ ions could re-enter the remaining Cu_{2-x}Se domains/NCs (as we showed in a previous work,³² substoichiometric Cu_{2-x}Se NCs are indeed able to incorporate Cu^+ ions in solutions, with the consequence that their stoichiometry and thus their plasmon properties can be modified). This would drastically lower the concentration of the free charge carriers and therefore quench the surface plasmon resonance of the remaining Cu_{2-x}Se phase. We tend to exclude the filling of Cu vacancies in the Cu_{2-x}Se domains by even a small number of Sn ions, as this should leave a trace in the Raman spectrum in the form of a peak/shoulder at 180 cm^{-1} (as shown in Figure 1c, bottom spectrum).

CONCLUSIONS

We have reported a case study on cation exchange reactions involving the two stable +2 and +4 oxidation states of Sn and Cu_{2-x}Se NCs. We demonstrated that both the intermediates and the final products of the exchange are intimately connected to the valence state of the entering species. More precisely, when large Sn^{2+} cations are involved in the exchange, orthorhombic SnSe NCs are produced with phase segregated $\text{Cu}_{2-x}\text{Se}/\text{SnSe}$ heterostructures as intermediates of the reaction. When small Sn^{4+} cations are instead chosen to replace Cu^+ ions in the Cu_{2-x}Se NCs, alloyed $\text{Cu}_{2-4y}\text{Sn}_y\text{Se}$ ($y \leq 0.33$) NCs are then formed, with a maximum incorporation of tin equal to $y = 0.33$. In both cases the shape and morphology of the initial NCs was retained. Interesting developments in this direction might involve the study of exchange reactions on other copper chalcogenide systems (Cu_{2-x}S , Cu_{2-x}Te) and on other cations that can exist in two stable oxidation states (for example Ge^{2+} and Ge^{4+}).

ASSOCIATED CONTENT

Supporting Information

Size distribution analysis of the Cu_{2-x}Se , $\text{Cu}_{2-4y}\text{Sn}_y\text{Se}$, and SnSe NCs, crystal structure of Cu_{2-x}Se and $\text{Cu}_{0.66}\text{Sn}_{0.33}\text{Se}$ phases and their site occupancy, EDS analysis of $\text{Cu}_{2-4y}\text{Sn}_y\text{Se}$ NCs, epitaxial relationships of $\text{Cu}_{2-x}\text{Se}/\text{SnSe}$ heterostructures, *in situ* approach, polycrystalline and cubic SnSe NCs in the cation exchange process with Sn^{2+} ions, control experiments with Sn^{4+} ions at high temperature, and X-ray diffraction study of Cu_{2-x}Se NCs films. This material is available free of charge via the Internet at <http://pubs.acs.org>.

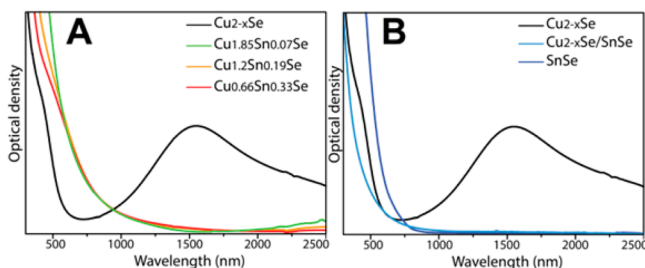


Figure 5. UV–vis–NIR absorption curve of solutions of (a) Cu_{2-x}Se and $\text{Cu}_{2-4y}\text{Sn}_y\text{Se}$ NCs; (b) Cu_{2-x}Se , $\text{Cu}_{2-x}\text{Se}/\text{SnSe}$, and SnSe NCs. All spectra are recorded on NCs dispersed in TCE.

■ AUTHOR INFORMATION

Corresponding Author

liberato.manna@iit.it

Author Contributions

Luca De Trizio and Hongbo Li contributed equally to this work.

Notes

The authors declare no competing financial interest.

■ ACKNOWLEDGMENTS

The research leading to these results has received funding from the European Union's Seventh Framework Programme FP7/2007-2013 under grant agreements 614897 (ERC Grant TRANS-NANO), 284486 (SCALENANO), and CNECT-ICT-604391 (Graphene Flagship). We thank Francesco De Donato for his help on the Cu_{2-x}Se NCs synthesis and Sergio Marras for help on the XRD experiments.

■ REFERENCES

- (1) Scholes, G. D. *Adv. Funct. Mater.* **2008**, *18*, 1157–1172.
- (2) Carbone, L.; Cozzoli, P. D. *Nano Today* **2010**, *5*, 449–493.
- (3) Talapin, D. V.; Lee, J.-S.; Kovalenko, M. V.; Shevchenko, E. V. *Chem. Rev.* **2010**, *110*, 389–458.
- (4) Xia, Y.; Xiong, Y.; Lim, B.; Skrabalak, S. E. *Angew. Chem., Int. Ed.* **2009**, *48*, 60–103.
- (5) Gao, Y.; Tang, Z. *Small* **2011**, *7*, 2133–2146.
- (6) Hines, D. a.; Kamat, P. V. *ACS Appl. Mater. Interfaces* **2014**, *6*, 3041–3057.
- (7) Nag, A.; Kovalenko, M. V.; Lee, J.-S.; Liu, W.; Spokoyny, B.; Talapin, D. V. *J. Am. Chem. Soc.* **2011**, *133*, 10612–10620.
- (8) Fayette, M.; Robinson, R. D. *J. Mater. Chem. A* **2014**, *2*, 5965–5978.
- (9) Beberwyck, B. J.; Surendranath, Y.; Alivisatos, A. P. *J. Phys. Chem. C* **2013**, *117*, 19759–19770.
- (10) Rivest, J. B.; Jain, P. K. *Chem. Soc. Rev.* **2013**, *42*, 89–96.
- (11) Son, D. H.; Hughes, S. M.; Yin, Y.; Alivisatos, A. P. *Science* **2004**, *306*, 1009–1012.
- (12) Jain, P. K.; Amirav, L.; Aloni, S.; Alivisatos, A. P. *J. Am. Chem. Soc.* **2010**, *132*, 9997–9999.
- (13) Luther, J. M.; Zheng, H.; Sadtler, B.; Alivisatos, A. P. *J. Am. Chem. Soc.* **2009**, *131*, 16851–16857.
- (14) Wark, S. E.; Hsia, C.-H.; Son, D. H. *J. Am. Chem. Soc.* **2008**, *130*, 9550–9555.
- (15) Justo, Y.; Sagar, L. K.; Flamee, S.; Zhao, Q.; Vantomme, A.; Hens, Z. *ACS Nano* **2014**, *8*, 7948–7957.
- (16) Li, W.; Zamani, R.; Ibáñez, M.; Cadavid, D.; Shavel, A.; Morante, J. R.; Arbiol, J.; Cabot, A. *J. Am. Chem. Soc.* **2013**, *135*, 4664–4667.
- (17) Li, H.; Zanella, M.; Genovese, A.; Povia, M.; Falqui, A.; Giannini, C.; Manna, L. *Nano Lett.* **2011**, *11*, 4964–4970.
- (18) Camargo, P. H. C.; Lee, Y. H.; Jeong, U.; Zou, Z.; Xia, Y. *Langmuir* **2007**, *23*, 2985–2992.
- (19) Li, H.; Brescia, R.; Krahne, R.; Bertoni, G.; Alcocer, M. J. P.; D'Andrea, C.; Scotognella, F.; Tassone, F.; Zanella, M.; De Giorgi, M.; Manna, L. *ACS Nano* **2012**, *6*, 1637–1647.
- (20) Miszta, K.; Dorfs, D.; Genovese, A.; Kim, M. R.; Manna, L. *ACS Nano* **2011**, *5*, 7176–7183.
- (21) Sadtler, B.; Demchenko, D. O.; Zheng, H.; Hughes, S. M.; Merkle, M. G.; Dahmen, U.; Wang, L.-W.; Alivisatos, A. P. *J. Am. Chem. Soc.* **2009**, *131*, 5285–5293.
- (22) Jain, P. K.; Beberwyck, B. J.; Fong, L.-K.; Polking, M. J.; Alivisatos, A. P. *Angew. Chem., Int. Ed.* **2012**, *51*, 2387–2390.
- (23) Smith, A. M.; Nie, S. *J. Am. Chem. Soc.* **2011**, *133*, 24–26.
- (24) Robinson, R. D.; Sadtler, B.; Demchenko, D. O.; Erdonmez, C. K.; Wang, L.-W.; Alivisatos, A. P. *Science* **2007**, *317*, 355–358.
- (25) Pietryga, J. M.; Werder, D. J.; Williams, D. J.; Casson, J. L.; Schaller, R. D.; Klimov, V. I.; Hollingsworth, J. A. *J. Am. Chem. Soc.* **2008**, *130*, 4879–4885.
- (26) Mocatta, D.; Cohen, G.; Schattner, J.; Millo, O.; Rabani, E.; Banin, U. *Science* **2011**, *332*, 77–81.
- (27) De Trizio, L.; Prato, M.; Genovese, A.; Casu, A.; Povia, M.; Simonutti, R.; Alcocer, M. J. P.; Andrea, C. D.; Tassone, F.; Manna, L. *Chem. Mater.* **2012**, *24*, 2400–2406.
- (28) Sahu, A.; Kang, M. S.; Kompch, A.; Notthoff, C.; Wills, A. W.; Deng, D.; Winterer, M.; Frisbie, C. D.; Norris, D. J. *Nano Lett.* **2012**, *12*, 2587–2594.
- (29) Beberwyck, B. J.; Alivisatos, A. P. *J. Am. Chem. Soc.* **2012**, *134*, 19977–19980.
- (30) Lesnyak, V.; George, C.; Genovese, A.; Prato, M.; Casu, A.; Ayyappan, S.; Scarpellini, A.; Manna, L. *ACS Nano* **2014**, *8*, 8407–8418.
- (31) Rivet, J.; Laruelle, P.; J, F.; Fichet, R. *Bull. Soc. Chim. Fr.* **1970**, 1667–1670.
- (32) Dorfs, D.; Härtling, T.; Miszta, K.; Bigall, N. C.; Kim, M. R.; Genovese, A.; Falqui, A.; Povia, M.; Manna, L. *J. Am. Chem. Soc.* **2011**, *133*, 11175–11180.
- (33) de Kergommeaux, A.; Faure-Vincent, J.; Pron, A.; de Bettignies, R.; Malaman, B.; Reiss, P. *J. Am. Chem. Soc.* **2012**, *134*, 11659–11666.
- (34) Parr, R. G.; Pearson, R. G. *J. Am. Chem. Soc.* **1983**, *105*, 7512–7516.
- (35) Kelly, A.; Groves, G. W. *Crystallography and Crystal Defects*; Longman: London, 1970.
- (36) Izquierdo-Roca, V.; Saucedo, E.; Ruiz, C. M.; Fontané, X.; Calvo-Barrio, L.; Álvarez-García, J.; Grand, P.-P.; Jaime-Ferrer, J. S.; Pérez-Rodríguez, A.; Morante, J. R.; Bermudez, V. *Phys. Status Solidi A* **2009**, *206*, 1001–1004.
- (37) Wang, J.-j.; Liu, P.; Seaton, C. C.; Ryan, K. M. *J. Am. Chem. Soc.* **2014**, *136*, 7954–7960.
- (38) Marcano, G.; Rincón, C.; López, S. a.; Sánchez Pérez, G.; Herrera-Pérez, J. L.; Mendoza-Alvarez, J. G.; Rodríguez, P. *Solid State. Commun.* **2011**, *151*, 84–86.
- (39) Fan, J.; Carrillo-Cabrera, W.; Antonyshyn, I.; Prots, Y.; Veremchuk, I.; Schnelle, W.; Drathen, C.; Chen, L.; Grin, Y. *Chem. Mater.* **2014**, *26*, 5244–5251.
- (40) Palosz, B.; Salje, E. J. *Appl. Crystallogr.* **1989**, *22*, 622–623.
- (41) Chandrasekhar, H. R.; Humphreys, R. G.; Zwick, U.; Cardona, M. *Phys. Rev. B* **1977**, *15*, 2177–2183.
- (42) Baumgardner, W. J.; Choi, J. J.; Lim, Y.-F.; Hanrath, T. *J. Am. Chem. Soc.* **2010**, *132*, 9519–9521.
- (43) Zhao, Y.; Pan, H.; Lou, Y.; Qiu, X.; Zhu, J.; Burda, C. *J. Am. Chem. Soc.* **2009**, *131*, 4253–4261.
- (44) Hessel, C. M.; P. Pattani, V.; Rasch, M.; Panthani, M. G.; Koo, B.; Tunnell, J. W.; Korgel, B. A. *Nano Lett.* **2011**, *11*, 2560–2566.
- (45) Hsu, S.-W.; Bryks, W.; Tao, A. R. *Chem. Mater.* **2012**, *24*, 3765–3771.
- (46) Luther, J. M.; Jain, P. K.; Ewers, T.; Alivisatos, A. P. *Nat. Mater.* **2011**, *10*, 361–366.
- (47) Comin, A.; Manna, L. *Chem. Soc. Rev.* **2014**, *43*, 3957–3975.
- (48) Xie, Y.; Riedinger, A.; Prato, M.; Casu, A.; Genovese, A.; Guardia, P.; Sottini, S.; Sangregorio, C.; Miszta, K.; Ghosh, S.; Pellegrino, T.; Manna, L. *J. Am. Chem. Soc.* **2013**, *135*, 17630–17637.